PHYSICAL REVIEW B **84**, 104507 (2011)

Vortex imaging and vortex lattice transitions in superconducting Sr_2RuO_4 single crystals

P. J. Curran, V. V. Khotkevych, and S. J. Bending
Department of Physics, University of Bath, Claverton Down, Bath BA2 7AY, United Kingdom

A. S. Gibbs, S. L. Lee, and A. P. Mackenzie
School of Physics and Astronomy, University of St. Andrews, St. Andrews KY16 9SS, United Kingdom
(Received 24 March 2011; revised manuscript received 26 July 2011; published 8 September 2011)

Scanning Hall probe microscopy has been used to study vortex structures in very-high-quality single crystals of the unconventional superconductor Sr_2RuO_4 ($T_c \cong 1.5$ K). In none of our samples do we find credible evidence for the existence of the spontaneous fields or chiral domains predicted for the expected time-reversal symmetry-breaking order parameter. Even in our highest-quality samples we observe very strong vortex pinning and anomalous broadening of vortex profiles. The best samples also exhibit a clear field-driven triangular to square vortex lattice transition at low fields, as predicted by extended London theory calculations. In stark contrast, slightly less well-ordered samples exhibit pronounced vortex chaining/banding that we tentatively attribute to an extrinsic source of disorder.

DOI: 10.1103/PhysRevB.84.104507 PACS number(s): 74.70.Pq, 74.25.Uv, 74.20.Rp, 74.62.En

I. INTRODUCTION

Unconventional superconductors are those in which Cooper pairs of electrons occur with unusual symmetries and are of major interest to researchers in the field because of the potential for discovering new binding mechanisms that are radically different to the electron-phonon interaction of conventional spin-singlet s-wave materials. Strontium ruthenate (Sr_2RuO_4) has a highly two-dimensional layered perovskite structure and was discovered to be a $T_c \cong 1.5$ K superconductor in 1994.[1] Theoretical suggestions that it was a good candidate for spin-triplet pairing mediated by ferromagnetic spin fluctuations emerged immediately due to the occurrence of ferromagnetism in the closely related compound $SrRuO_3$.[2] The results of several experiments have subsequently supported this picture. The strong suppression of T_c by nonmagnetic impurities indicated an unconventional non-s-wave pairing[3] and subsequent NMR measurements of the Knight shift[4] and polarized neutron scattering[5] provided further strong evidence for spin-triplet superconductivity. For triplet pairing p-wave order is most likely, although higher-order odd pairing is also possible. Five possible unitary order parameters are consistent with the D_{4h} point group symmetry of Sr_2RuO_4 (Ref. 6). The detection of the spontaneous generation of flux in μSR measurements below T_c (Ref. 7) and later polar Kerr effect measurements in the superconducting state[8] pointed to the presence of time-reversal symmetry breaking (TRSB) in this material. This, in turn, implicates the two-component chiral order parameter with d vector $d = \Delta_0(k_x \pm ik_y)\hat{z}$. More recent phase-sensitive measurements on Sr_2RuO_4 superconducting quantum interference devices (SQUIDs)[9] and Josephson junctions[10] have supported the p-wave order-parameter scenario, although the latter authors needed to invoke complex static and dynamic chiral domains to explain their data.

Since the Cooper pair carries angular momentum in the p-wave pairing state, another characteristic signature of it would be the presence of spontaneous currents anywhere that translational symmetry is broken (e.g., at sample edges and chiral domain walls). These spontaneous currents should form on a length scale of the coherence length, ξ, and, although they will be screened by counterpropagating currents over the longer length scale of λ, should still generate readily detectible magnetic fields.[11,12] It is surprising then that several scanning SQUID[13–15] and scanning Hall probe[16] microscopy studies have failed to find convincing evidence for spontaneous currents anywhere in high-quality Sr_2RuO_4 single crystals at $H = 0$.

Time-dependent two-component Ginzburg-Landau (TCGL) simulations[17] suggested that vortex ordering phenomena in a system of chiral domains in an applied c-axis magnetic field might also reflect the underlying domain structure. In their simulations these authors found that domain walls weakly pin the magnetic flux and vortices preferentially enter domains of one chirality and eventually move domain walls to expel the reverse domain. They even observed the formation of a few 4π vortices at the boundary of their sample. To date none of these predictions has been experimentally confirmed. As well as possible interactions with chiral domain walls, qualitative differences in vortex behavior are expected in superconductors with unconventional order parameters that can yield independent insights into the underlying superconducting state. Consequently, identifying unconventional vortex behavior was another major goal of this work, in addition to the search for spontaneous "chiral" supercurrents. The observation of a stable square vortex lattice over most of the H-T phase space by neutron diffraction[18] and μSR[19] experiments is an example of such unconventional behavior and is in agreement with the predictions of TCGL calculations that include Fermi surface and order-parameter anisotropies.[20]

The lack of real-space experimental evidence for chiral currents and domain walls which are linked to the observed TRSB in other measurements is a major challenge for this field. Indeed, several recent reviews have been devoted to this issue and the establishment of upper and lower bounds on possible domain sizes.[15,21,22] It is against this rather uncertain background that the series of scanning Hall probe microscopy experiments described here was conducted.

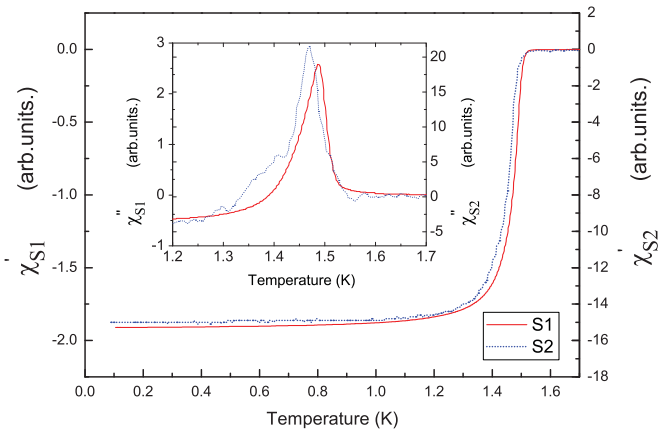

FIG. 1. (Color online) Real part of ac susceptibility data measured through the critical temperature of the two crystals studied here. The inset shows the imaginary part of the ac susceptibility near T_c.

II. EXPERIMENTAL METHOD

Superconducting single crystals were grown using the floating-zone technique with Ru self-flux in a commercial image furnace[23] and annealed in air (1500 °C for 3 days) to remove lattice defects and reduce vortex pinning.[24] Scanning Hall probe imaging has been performed on many different crystals from different growth batches. Here we present results on two samples, grown under nominally identical conditions in different growth batches, that illustrate the extremes of behavior observed. We attribute the pronounced differences in the vortex structures observed in the two crystals to slightly different Ru compositions in the two growth ingots. Figure 1 shows the real and imaginary components of ac susceptibility measurements on the two samples presented here. Defining T_c as the point when χ' falls below 10% of the low temperature susceptibility, we find a spread in T_c values from 1.485 K and 1.500 K for all the different samples studied. Any broadening of the transition for each individual sample is below our measurement resolution (<0.01 K). Figure 1 shows that sample 2 has a slightly lower T_c than sample 1 and the imaginary component of its susceptibility, χ'', shows a clear shoulder in the range $T = 1.3$–1.4 K, indicative of the presence of small amounts of a second phase.

The scanning Hall probe microscope (SHPM) head used to image vortices was custom designed to fit onto the cold plate of a commercial Oxford Instruments Heliox ^{3}He refrigerator. The scanner head was based around a microfabricated GaAs/AlGaAs heterostructure chip containing integrated magnetic field and topography sensors. Electron beam lithography and wet chemical etching were used to define a 600 × 600-nm active area Hall sensor in the two-dimensional electron gas approximately 5 μm from the corner of a deep mesa etch, which was coated with a thin Au layer to act as an integrated scanning tunneling microscopy (STM) tip. The sample was first approached toward the sensor until tunneling was established and then retracted about 100 nm to allow rapid scanning without height feedback. The Hall probe subtended an angle of about 1° with the sample plane so that the STM tip was always the closest point to the surface, and the Hall sensor was typically ≈500 nm above the sample during imaging.

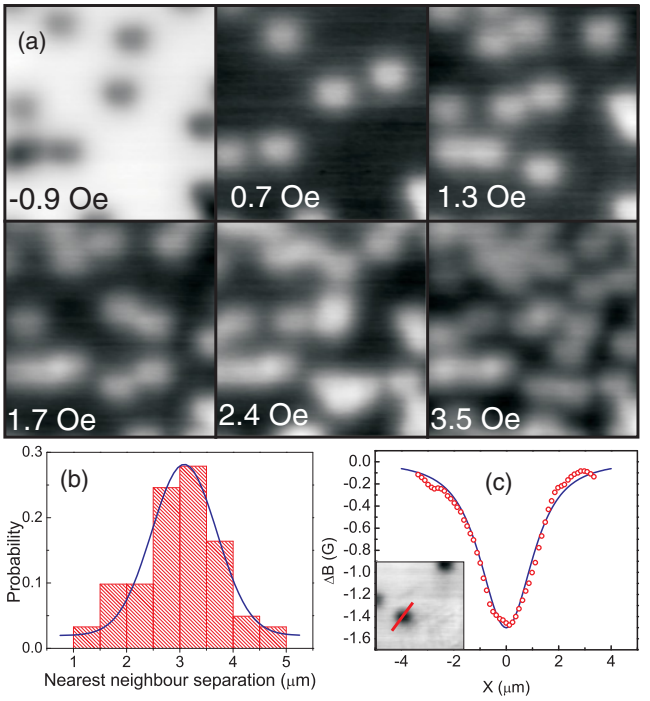

FIG. 2. (Color online) (a) SHPM images captured parallel to the a-b face of sample 1 after field cooling from above T_c in the indicated applied fields ($H \| c$ axis). Scan size ≈14 × 14 μm; $T = 330$ mK. (b) Statistical distribution of nearest-neighbor vortex distances for the image at $H = 3.5$ Oe. The solid line is a Gaussian fit to the data (mean = 2.95 μm, $\sigma = 0.8$ μm). (c) Line profile across a well-isolated vortex in an image captured at $H = -0.2$ Oe (see inset). The solid line is a fit to the Clem variational model with $\xi_v = 66$ nm, $\lambda = 165$ nm, $w = 600$ nm, and $h = 1.26$ μm.

The maximum scan field was ≈14 × 14 μm at 300 mK and was only very weakly temperature dependent for the range explored here, $0.3 \leqslant T \leqslant 1.5$ K. A more detailed description of the instrument and scanning technique is given elsewhere.[25]

III. RESULTS

A. Sample 1

Sample 1 has the highest critical temperature ($T_c = 1.5$ K) and a very sharp superconductor-normal transition and is expected to exhibit the properties of a very highly ordered Sr_2RuO_4 single crystal. Figure 2(a) shows a family of SHPM images captured parallel to the a-b crystal face, after field cooling to $T \approx 300$ mK from above T_c ($H \| c$ axis) in various cooling fields spanning $H = 0$. A detailed analysis reveals no credible evidence for the presence of spontaneous currents/fields in these images for $H \approx 0$, nor indeed in any other of the many different regions of the sample explored. Hence, we conclude that, if they are present, chiral domain walls are not observable within our experimental resolution. In practice the STM-tracking technique used here prevents us from mapping images across the edge of the crystal, so we are unable to draw any conclusions about the possible presence of spontaneous edge currents.

Recent scanning Hall[16] and SQUID[13,15,26] microscopy images from Sr_2RuO_4 single crystals have been interpreted

in terms of vortex coalescence arising, possibly, from a weak long-range vortex attraction at low fields. A careful analysis of all the images captured on sample 1 revealed no statistically significant evidence for clustering in the vortex patterns at low applied fields [Fig. 2(a)]. To illustrate this point, Fig. 2(b) presents a statistical analysis of nearest-neighbor vortex-vortex distances after Delaunay triangulation of the image at −3.5 Oe. These data are well described by a single Gaussian fit, with no evidence for a second peak at low fields which would indicate the presence of vortex clustering.

Figure 2(c) shows a fit to the profile across a well-isolated vortex measured at $H = -0.2$ Oe (see inset) based on the Clem variational model (Ref. 27) modified to account for surface screening effects using an approach due to Kirtley *et al.* (Ref. 14) and assuming a variational coherence length $\xi_v = 66$ nm, $\lambda = 165$ nm, and an active Hall probe width, w, of 600 nm:

$$B(x,y,z) = \frac{\phi_0}{w^2}\int_{y-\frac{w}{2}}^{y+\frac{w}{2}}\int_{x-\frac{w}{2}}^{x+\frac{w}{2}}\int_0^\infty \times \frac{K_1(\sqrt{k^2+\lambda^{-2}}\xi_v)}{2\pi\lambda(\sqrt{k^2+\lambda^{-2}}+k)K_1(\xi_v/\lambda)} \times J_0(k\sqrt{x'^2+y'^2})\exp(-kz)kdkdx'dy', \quad (1)$$

where z is the sensor-sample separation. The quality of the fit is clearly excellent, confirming that this vortex contains a single flux quantum. The scan height above the surface of the superconductor has been treated here as a fit parameter and is found to be 1.26 μm. This is very much larger than expected for our system (≈0.5–0.75 μm) and, if true, would make it virtually impossible to resolve the square vortex lattice at high fields (>20 Oe), shown later. It appears, therefore, that there is some as-yet-unexplained vortex broadening that is not included in the Clem model. As we increase the applied field ($H \| c$ axis) above 4 Oe we witness the emergence of first triangular and then square vortex order out of the essentially random low-field distributions shown in Fig. 2(a). This is illustrated in Fig. 3, where we present direct SHPM images in tandem with their self-correlation (SC) plots, which are particularly useful tools for characterizing vortex order. The first image at 3.9 Oe shows a rather random distribution of weakly pinned vortices, a fact reflected in the broadly featureless SC plot. However, upon increasing the field to just 5.4 Oe we start to see a pronounced degree of triangular order as evidenced by the hexagon of six bright spots in the center of the SC plot (cf., also the region of hexagonal mesh superimposed on the raw vortex image). This reflects the emergence of the usual triangular Abrikosov vortex lattice driven by vortex-vortex repulsion. Surprisingly, the triangular lattice is lost again at 6.8 Oe and there appears to be some competition between two different forms of order. Indeed, for yet higher applied fields we find a transition to a square vortex lattice, albeit a fairly defected one, which is almost complete in the rather well-ordered image shown at 12.7 Oe. This observation is in agreement with the results of neutron diffraction measurements at somewhat higher fields.[18,28]

Figure 4(a) shows that we observe a weakly disordered square vortex lattice with the same orientation as we increase

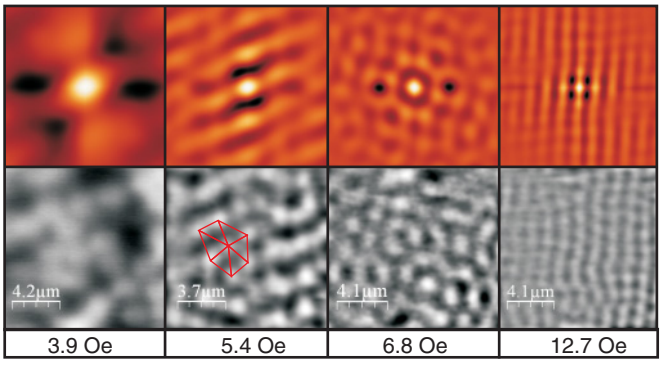

FIG. 3. (Color online) SHPM images captured parallel to the a-b face of sample 1 after field cooling from above T_c in the indicated applied fields ($H \| c$ axis). Scan size ≈14 × 14 μm; $T = 330$ mK. The top row shows self-correlation plots of the raw images in the bottom row (vortices are white).

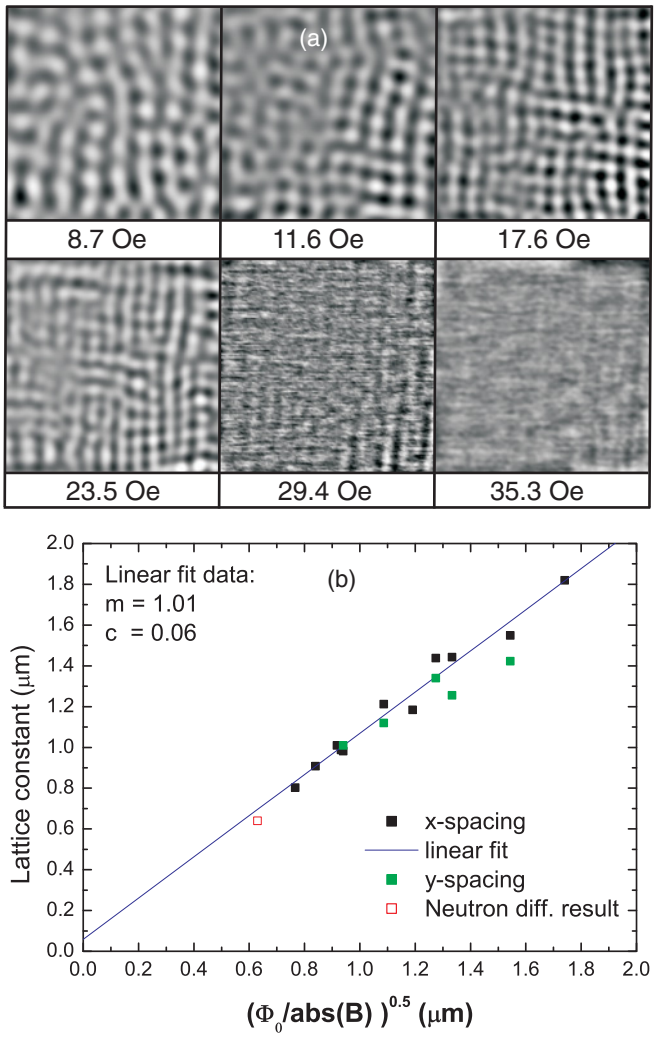

FIG. 4. (Color online) (a) SHPM images captured parallel to the a-b face of sample 1 after field cooling from above T_c in the indicated applied fields ($H \| c$ axis). Scan size ≈14 × 14 μm; $T = 330$ mK. (b) The square lattice spacing measured in the x- and y-scan directions plotted versus $(\Phi_0/|B|)^{0.5}$. The solid line is a linear regression fit to these data. Also shown (open square) is the lattice spacing estimated from neutron diffraction experiments at $H = 50$ Oe (Ref. 18).

the field further up to about 35 Oe, where we lose the ability to resolve discrete vortices. Note that the lattice periodicity is clearer in the fast x-scan direction than in the slow y-scan direction at high fields due to the dominant low-frequency noise in our Hall sensors. This gives the impression of vertically aligned vortex stripes or chains but after averaging several adjacent y lines the underlying periodicity is revealed. Figure 4(b) shows plots of the experimentally estimated lattice spacing for both x- and y-scan directions plotted as a function of $(\Phi_0/|B|)^{0.5}$. Linear regression of these data yields a fit with slope $m = 1.01$ and y-axis intercept $c = 0.06\ \mu$m, in excellent agreement with the expected line of unity slope passing through the origin for a perfect square vortex lattice. Also plotted on the figure is the lattice spacing inferred from neutron diffraction data at the lowest field measured.[18] The fact that the lattice spacing in both x- and y-scan directions lies on the same fit line, within the resolution of our experiment, also appears to rule out rectangular ordering, at least in fields up to 35.3 Oe.

B. Sample 2

The lower quality sample 2 ($T_c \cong 1.5$ K with a broader superconductor-normal transition) displays markedly different behavior to sample 1, even though both crystals were grown under the same nominal conditions. Figure 5 shows two composites of several individual images captured at $H = 2.4$ Oe (a) and 15.7 Oe (b). At low fields [Fig. 5(a)] we see that vortices occupy quasiperiodic chain structures that

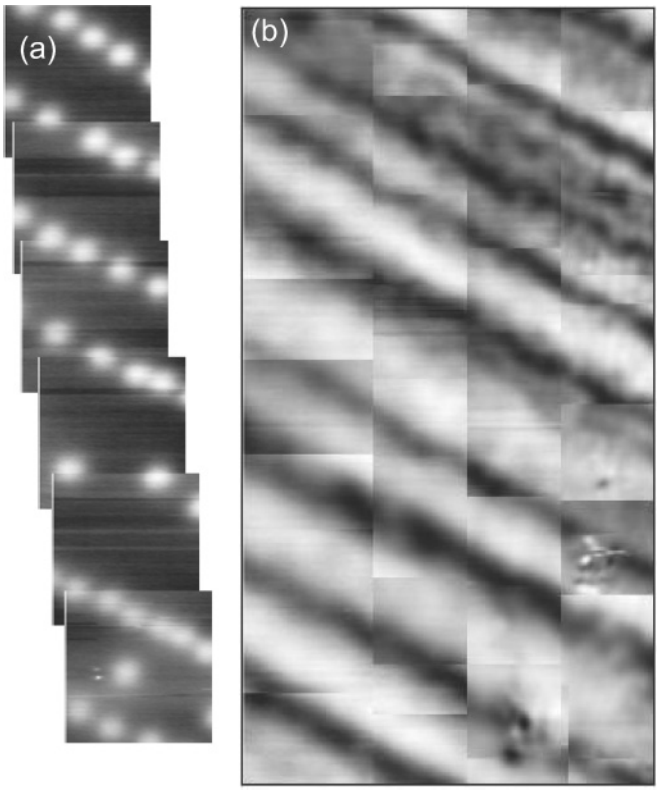

FIG. 5. Composite SHPM images captured parallel to the a-b face of sample 2 after field cooling from above T_c in applied fields ($H \| c$ axis) (a) $H = 2.4$ Oe ($\approx 20 \times 70\ \mu$m) and (b) $H = 15.7$ Oe ($\approx 45 \times 70\ \mu$m). $T = 330$ mK.

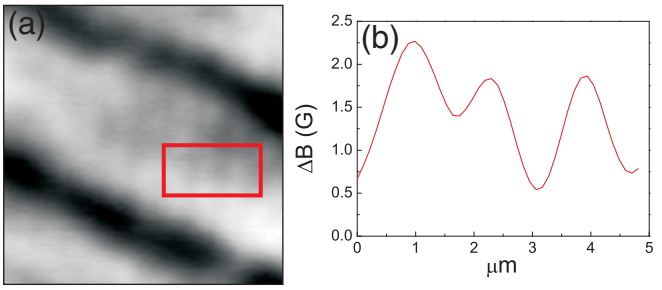

FIG. 6. (Color online) (a) SHPM image captured parallel to the a-b face of sample 2 after field cooling from above T_c in $H = 16$ Oe ($H \| c$ axis). Scan size $\approx 14 \times 14\ \mu$m; $T = 330$ mK. (b) Average of the x-scan lines in the region indicated in (a) showing the presence of vortex chains within the bands.

lie at 23° (67°) with respect to the scan axes. The chains are reasonably regularly spaced with a period of $\approx 10\ \mu$m and are quite inhomogenously populated. At higher fields [Fig. 5(b)] these chains expand and form irregular bands.

Figure 6(a) details one of the panels from the composite shown in Fig. 5(b) captured at $H = 16$ Oe. Vertical chains are clearly visible parallel to the y-scan direction within the bright white vortex bands. Figure 6(b) shows the average of a set of x-scan lines in the rectangular region indicated in Fig. 6(a), clearly revealing the presence of these vertical vortex chains. We believe that these short periodicity chains arise due to the same electronic anisotropies that lead to the formation of the square lattice in sample 1.

Figure 7 captures the evolution from sparse chains to bands over a broad range of fields until we begin to lose contrast for $H > 51$ Oe. Note that the flux expelling areas (black) are gradually squeezed smaller and smaller by increasing the number of vortices in the chains/bands. Note also that the grayscale of the images at high fields is much less than the peak contrast of a single vortex as well as the magnitude of

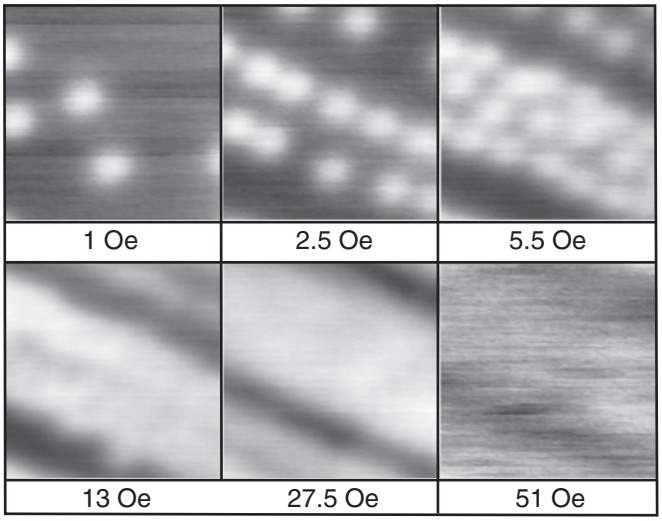

FIG. 7. SHPM images captured parallel to the a-b face of the same region of sample 2 after field cooling from above T_c in the indicated applied fields ($H \| c$ axis). Vortices are white; scan size $\approx 14 \times 14\ \mu$m; $T = 330$ mK. Grayscale (ΔB) spans 1.98, 2.13, 1.89, 2.7, 2.55, and 0.89 G, respectively.

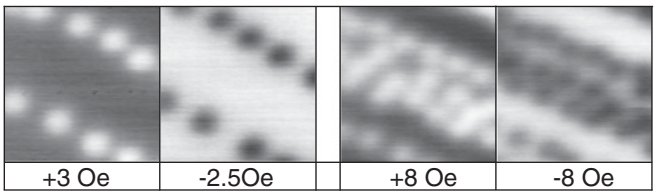

FIG. 8. SHPM images captured parallel to the a-b face of the same region of sample 2 after field cooling from above T_c in the indicated applied fields ($H \| c$ axis). Scan size $\approx 14 \times 14$ μm; $T =$ 330 mK.

the applied field. Hence, we conclude that vortices are present everywhere, but have a lower density on the dark strips than in the bright bands between them.

Theoretical simulations based on time-dependent TCGL theory in a system of chiral order-parameter domains[17] predict that vortices preferentially enter those domains with a matching chirality; that is, up and down vortices preferentially penetrate different regions. If we assume that the order parameter is not influenced by small applied fields, an easy test of this prediction is to reverse the field and observe the preferred locations of vortices of opposite sign (cf., Fig. 8). In all cases we see no difference in the preferred vortex locations within the resolution of a single vortex (<2 μm), which seems to rule out the possibility that the chain/band structure we see reflects an underlying chiral domain structure. Finally we note the interesting tendency for low-field chains to be positioned along one edge of the emerging bands, not in the center, as one might expect. As a consequence, the vortex bands tend to fill in from one side, and this evolution starts at the same side for both up and down vortices.

Assuming that the formation of these vortex chains/bands is related to the presence of some form of anisotropic pinning potential, it is interesting to study their temperature dependence. The increased thermal energy at higher temperatures should allow vortices to overcome pinning potentials, freeing them up to move closer to their equilibrium configurations. Figure 9 presents a sequence of vortex images captured at different temperatures after field cooling to 327 mK in $H = 2.4$ Oe. As the temperature is increased we see that the mean vortex-vortex spacing increases [presumably due to the increasing penetration depth, λ(T)] and the chains broaden into lower-density bands. Close to T_c at $T = 1.317$ K we see pronounced triangular vortex ordering, with a complete loss of vortex contrast for $T > 1.4$ K.

IV. DISCUSSION

One of the key signatures of a chiral p-wave order parameter, which has so far eluded all magnetic imaging experiments, is the presence of spontaneous currents (fields) at sample edges, chiral domain boundaries, or crystalline imperfections. The use of STM-based height control in our scanning system prevents us from imaging across the edge of the crystal. However, we find no credible evidence for spontaneous fields that we could attribute to either chiral domain walls or crystal defects anywhere within our samples at very low applied fields. Figure 10 presents a simulation of the stray fields we would expect to measure based on the fitting

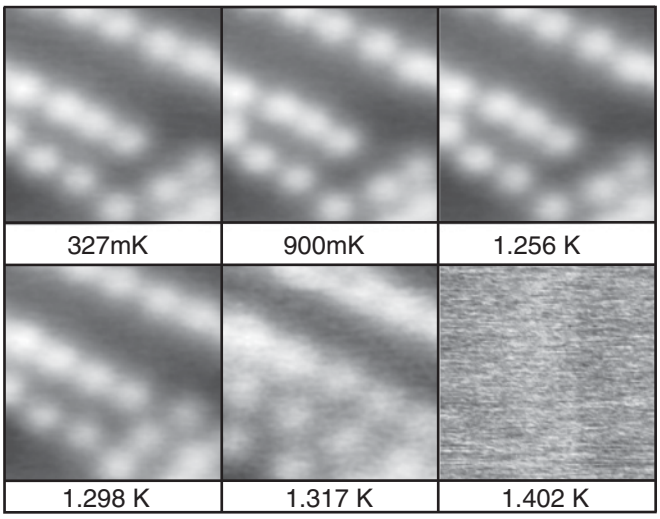

FIG. 9. Temperature dependence of SHPM images captured parallel to the a-b face of the same region of sample 2 after field cooling from above T_c in $H = 2.4$ Oe ($H \| c$ axis). Scan size $\approx 14 \times 14$ μm.

protocol of Bluhm[12] to describe the numerical solutions of the inhomogeneous London equation for spontaneous currents at a infinite chiral domain wall given by Matsumoto and Sigrist.[11] Here we have assumed a scan height of $z = 0.8$ μm and surface screening has again been accounted for using the approach due to Kirtley *et al.*[14] We arrive at the result for the normal component of magnetic field at a chiral domain boundary given by Eq. (2):

$$B_z(x,z) = \frac{B_0}{1-\tilde{\xi}^2/\tilde{\lambda}^2}\frac{1}{2\pi w} \times \int_{x_i-\frac{w}{2}}^{x_i+\frac{w}{2}} \int_0^{100} \left(\frac{2k}{1/\tilde{\lambda}^2+k^2} - \frac{2k}{1/\tilde{\xi}^2+k^2}\right) \times \left(\frac{\sqrt{k^2+\lambda^2}}{|k|+\sqrt{k^2+\lambda^2}}\right) 2\sin(kx) e^{(-|k|z)} dk dx. \quad (2)$$

We have assumed $\lambda = 150$ nm and $\xi = 66$ nm and an active Hall probe width of 600 nm, and adopted Bluhm's fit parameters $\tilde{\lambda} = 2.2\xi$ and $\tilde{\xi} = 1.5\xi$. B_0 is an additional fitting parameter introduced by Bluhm which he took to be 87 G in order to match the field scale of the numerical calculations. In Fig. 10 we plot the calculated chiral domain fields for various choices of B_0, and show that the estimated signal would fall below the noise floor of our measurements ($\approx$0.04 G) if, in practice, B_0 was about 36 times smaller ($<$2.4 G).

Furthermore, upon field-cooling in small applied fields we find no evidence for enhanced vortex penetration along chiral domain walls or the preferential occupation of domains of a given chirality, although these phenomena may only become pronounced in zero field-cooled experiments. Very-low-field vortex structures were typically highly disordered in even the highest quality samples [cf., Fig. 2(a)], and repeated images after field cooling through T_c in the same field at the same location invariably revealed that the majority of vortices occupied the same locations, suggesting a fairly low density of rather strong pinning sites. Vortex pinning typically

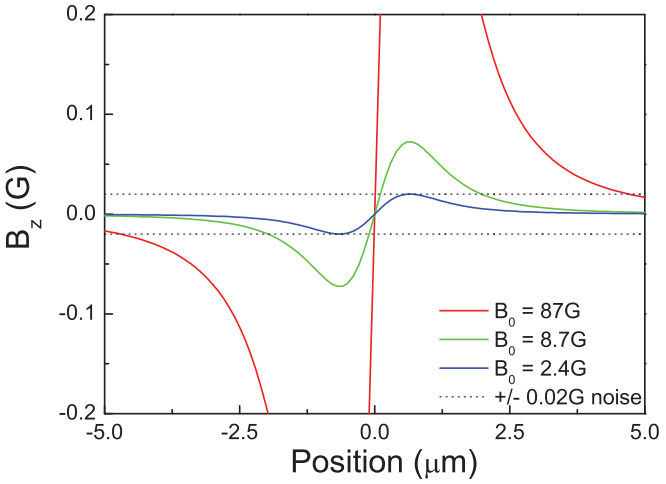

FIG. 10. (Color online) Simulations of the stray field along line scans perpendicular to an infinite chiral domain boundary (x-axis origin is at the center of the wall) based on the fitting protocol of Bluhm (Ref. 12), who took B_0 to be 87 G. The fields have been calculated for various choices of B_0 and the noise floor of our measurements ($\Delta B \approx 0.04$ G) is indicated by horizontal dashed lines.

occurs anywhere that the superconducting order parameter is suppressed which, in a p-wave superconductor, could occur due to elastic scattering at crystal defects. If this is indeed the origin of the strong pinning forces it is somewhat at odds with other measurements (e.g., de Haas-van Alphen)[29] which find an extremely long carrier mean free path of the order of ≈ 1 μm in our best samples. Given that lattice imperfections are predicted to give rise to spontaneous fields we speculate that there could be a link between these strong pinning centers and the "broad distribution of fields from a dilute distribution of sources" detected by the μSR experiments.[7]

It is possible that our field-cooling experimental protocol has suppressed the chiral domain structure in measurements at higher fields. An applied field splits the degeneracy of the $J_z = \pm 1$ chiral states and might result in the formation of a predominantly single domain state.[17] This would dramatically reduce our chances of imaging a domain wall in the relatively small field of view available. However, we have performed several experiments in nominally zero field (after applying a small field to compensate for Earth's field), which also yielded no evidence for domains. Kallin and Berlinsky[21] have carefully analyzed all the available experimental data on Sr_2RuO_4 with a view to establishing upper and lower bounds on domain sizes. Estimated values vary dramatically from <1 μm[10] to ≈ 50 μm.[8] Given that there is still much debate about the expected 3D domain structure,[15] possible domain dynamics,[8,10] and the expected magnitude of spontaneous fields,[30] it is premature to draw very robust conclusions from our images. Suffice it to say that we have not been able to observe chiral domain walls at length scales spanning 0.8 to ≈ 14 μm with minimum detectable fields ≈ 0.04 G at time scales slower than ≈ 1 s (the time taken to scan a single line of the image).

The spatial resolution of SHPM is limited either by the lateral size of the Hall probe active area or the sample-sensor separation, whichever is greater. In our case we estimate that the active width of our square Hall probe is ≈ 600 nm and sample-sensor spacing is likely to be the dominant limiting factor. While the scan height of 1.26 μm used to fit the vortex profile in Fig. 2(c) is not at first sight entirely unreasonable, on the same day with the same sample-sensor spacing we were able to resolve the square vortex lattice at $H_z \approx 35$ Oe. This clearly sets an upper bound on the actual scan height of $h \leqslant 0.8$ μm, the vortex lattice spacing at this field. If we fix the scan height in the model to 0.8 μm, we find that we need to increase the London penetration depth to ≈ 500 nm to get a good fit, three times the accepted value of 165–190 nm reported in the literature. It appears, therefore, that there is some as-yet-unexplained broadening in our vortex images that is not accounted for in the Clem model. We speculate that this could either be related to the presence of a free surface (e.g., some form of surface scattering) or the traps that act as strong vortex pinning centers. Alternatively, it might reflect motional broadening due to vortex fluctuations about their pinning sites.

Vortex "coalescence" in Sr_2RuO_4 has been reported in previous scanning SQUID imaging experiments.[13,15,26] Since the Ginzburg-Landau parameter for Sr_2RuO_4 $\kappa = \lambda/\xi \approx 2.5$ it represents a fairly weakly type II superconductor. Hence, it is not inconceivable that the vortex-vortex interaction has a long-range attractive component as observed in superconductors with κ close to $1/\sqrt{2}$ by Bitter decoration many years ago[31] or within the two-band "type 1.5" scenario proposed recently for very clean MgB_2 single crystals.[32] In this situation a nearest-neighbor analysis of vortex separations will exhibit at least two peaks, one reflecting the intervortex spacing within clusters and one reflecting the intercluster spacing. The nearest-neighbor separation histogram for the highly ordered sample 1 in Fig. 2(b) can be well fitted by a single Gaussian curve and we find no evidence for clustering over the length scale of our field of view (≈ 14 μm). In contrast, a similar analysis for images such as those shown in Fig. 5(a) for the slightly more disordered sample 2 would show a second peak corresponding to the chain separation. However, we believe that these chains have an extrinsic origin as discussed below, and are not intrinsic to the physics of Sr_2RuO_4.

Vortices in an isotropic s-wave superconductor are expected to arrange in a hexagonal lattice. It is, however, well established that Fermi surface and order-parameter anisotropies can lead to other forms of vortex ordering, that is, a square vortex lattice.[6,33] Heeb and Agterberg[20] have used an extended London theory ($\kappa \gg 1$) for a two component p-wave order parameter, to investigate the ground state vortex structure in Sr_2RuO_4 as a function of Fermi surface anisotropy, $|\nu| \ll 1$, and applied field. They predict a continuous triangular $\rightarrow$ rectangular $\rightarrow$ square field-driven transition, with switching fields that are strongly dependent on the value of ν. Earlier μSR[34] and SANS[18] measurements have clearly demonstrated the existence of a square vortex lattice at high magnetic fields. The SANS measurements found square ordering everywhere the lattice could be resolved ($H_z > 50$ Oe) and we believe that the hexagonal to square transition shown in Fig. 3 for the field range 5.4 Oe $\leqslant$ Hz $\leqslant$ 12.7 Oe is the first experimental evidence that the vortex lattice in Sr_2RuO_4 does indeed reorder at low fields. The extended London theory of Heeb and Agterberg assumes that $\kappa \gg 1$ and hence does not strictly apply to Sr_2RuO_4 ($\kappa \approx 2.5$) and we are unable to draw

any quantitative conclusions about the magnitude of ν. Our observed crossover is at considerably lower fields than in the high κ ($\kappa = 5, \kappa = 25$) simulations of Heeb and Agterberg, but the same authors note that the crossover to a square lattice would occur at lower applied fields and lower anisotropies for a superconductor with smaller κ.

Finally, we discuss the quasiperiodic chaining/banding of vortices observed in sample 2. Some of the images shown in Figs. 6–9 appear, at least superficially, similar to previous scanning SQUID data from Ref. 13, where the possibility of vortex "coalescence" associated with a chiral domain structure is suggested. Several observations lead us to believe that this is not the case in our experiments on this sample. First, the "domain" boundaries we observe are fixed spatially and independent of cooling cycle, whereas one would expect the locations of chiral domain walls to vary randomly after repeatedly field cooling through T_c. We also see no qualitative change to the quasiperiodic structure after cooling in quite high fields of either sign ($|H_z| \approx 50$ Oe) when one would expect the degeneracy of domains to be lifted, favoring a single domain structure. It is possible that the chiral domain walls are strongly pinned, for example, at lattice defects, but again we see no evidence for spontaneous currents (fields) at very low inductions (cf., Fig. 7) that would indicate their presence. Instead, we speculate that the chaining/banding phenomenon is an extrinsic effect related to details of the growth of single crystal samples. It is well established that Ru lamellae often arise from eutectic solidification during Sr_2RuO_4 crystal growth.[35] These structures can vary greatly in size and orientation but frequently have dimensions and spacings comparable to the period and width of chains/bands observed here. It is possible, therefore, that type I superconducting Ru lamellae are leading to local flux exclusion and a modulation of the vortex density in the way we observe. Ruthenium has $T_c \approx 0.5$ K and a critical field, $H_c = 69$ G. This critical field is consistent with the observation that the banding is almost fully suppressed above $H_z = 51$ Oe as shown in Fig. 7. However, the critical temperature is too low to explain the chains/bands seen in Fig. 9 at $T = 0.9$ K and above. It is well known, however, that there is an interface phase between the lamellar Ru and Sr_2RuO_4 with a much higher critical temperature of $T_c \approx 3$ K[35] and it is possible that this is responsible for the effects we see at elevated temperatures. However, the expected signal is not present in ac susceptibility measurements and it would be hard to explain the complete loss of magnetic contrast far below 3 K (≈1.4 K, Fig. 9) if this were the case. While the T_c differences could be consistent with the presence of a second phase in the crystal, there are no further signaling features at 0.5 K or 3 K that indicate its presence. In addition, we have been unable to find traces of a 0.5 K Ru phase in heat capacity or bulk magnetometry measurements, and these samples still exhibit very long carrier mean free paths (≈1 μm) in de Haas-van Alphen measurements so the chaining/banding behavior of vortices is very difficult to explain in terms of these two known phases. Last, we note that a careful analysis of the series of images illustrated in Fig. 7 reveals that the chains of vortices evolve asymmetrically into bands as the field is increased. Initial vortex entry occurs at one edge of the band, not in the center, as one might expect, and the band then fills out toward the low-density direction, regardless of whether applied fields are positive or negative. A similar effect can be observed in the higher-temperature images of Fig. 9. This suggests an asymmetric pinning potential for the vortices, possibly having a sawtoothlike profile along a direction perpendicular to the chains. In addition to these "extrinsic" effects, we have also detected behavior that we attribute to the "intrinsic" underlying physics of Sr_2RuO_4 in sample 2. The chaining of vortices within the bands illustrated in Fig. 6(a) presumably arises from the same electronic anisotropies giving rise to a square vortex lattice in sample 1. However, the measured periodicity of these chains at $H_z = 16$ Oe [Fig. 6(b)] is nearly 40% larger than the expected square lattice spacing at this field [cf., Fig. 4(b)]. We presume that this is the result of partial flux screening by the source of extrinsic disorder responsible for the diagonal banding. At medium fields (5.5 Oe in Fig. 7) there appears to be a degree of triangular ordering in vortex images but this cannot be concluded with any certainty since vortex structures are so heavily influenced by the extrinsic disorder. Finally, we note the transition from chainlike to hexagonal vortex order as the temperature is increased in Fig. 9. This suggests that vortex-vortex interactions start to dominate over the disorder potentials at high temperatures. In addition, the hexagonal ordering close to T_c is consistent with μSR measurements at $H_z = 150$ Oe, which appear to show a temperature-driven square → hexagonal lattice transition.[34]

V. CONCLUSION

We have performed scanning Hall probe magnetic imaging of several high-quality Sr_2RuO_4 single crystals. In all cases we have failed to detect any magnetic signals that we can credibly attribute to the spontaneous magnetization predicted for a TRSB order parameter. Low field vortex distributions are consistent with the existence of strong pinning and we speculate that these pinning sites could be linked to the dilute distribution of field sources detected in μSR experiments.

We find no evidence of vortex clustering in our most highly ordered samples at low fields, but the field profiles of isolated vortices do reveal an unidentified source of broadening. We have resolved a field-driven triangular → square vortex lattice transition in our highest ordered samples at low fields, consistent with extended London theory calculations for a p-wave order parameter.

Slightly less well-ordered samples exhibit pronounced vortex chaining/banding, which we attribute to an extrinsic source of disorder, possibly the presence of Ru lamellae. The vortex-vortex interaction appears to dominate over this disorder potential at high temperatures close to T_c, where pronounced hexagonal vortex ordering is recovered.

ACKNOWLEDGMENTS

We acknowledge useful discussions with D. F. Agterberg and J. F. Annett. This work was supported by the Engineering and Physical Sciences Research Council (EPSRC) in the United Kingdom under Grant Nos. EP/D034264/1 and EP/E039944/1.

[1]Y. Maeno, H. Hashimoto, K. Yoshida, S. Nishizaki, T. Fujita, J. G. Bednorz, and F. Lichtenberg, Nature (London) **372**, 532 (1994).
[2]T. M. Rice and M. Sigrist, J. Phys. Condens. Matter **7**, L643 (1995).
[3]A. P. Mackenzie, R. K. W. Haselwimmer, A. W. Tyler, G. G. Lonzarich, Y. Mori, S. Nishizaki, and Y. Maeno, Phys. Rev. Lett. **80**, 161 (1998).
[4]K. Ishida, H. Mukuda, Y. Kitaoka, K. Asayama, Z. Q. Mao, Y. Mori, and Y. Maeno, Nature (London) **396**, 658 (1998).
[5]J. A. Duffy, S. M. Hayden, Y. Maeno, Z. Mao, J. Kulda, and G. J. McIntyre, Phys. Rev. Lett. **85**, 5412 (2000).
[6]A. P. Mackenzie and Y. Maeno, Rev. Mod. Phys. **75**, 657 (2003).
[7]G. M. Luke, Y. Fudamoto, K. M. Kojima, M. I. Larkin, J. Merrin, B. Nachumi, Y. J. Uemura, Y. Maeno, Z. Q. Mao, Y. Mori, H. Nakamura, and M. Sigrist, Nature (London) **394**, 558 (1998).
[8]J. Xia, Y. Maeno, P. T. Beyersdorf, M. M. Fejer, and A. Kapitulnik, Phys. Rev. Lett. **97**, 167002 (2006).
[9]K. D. Nelson, Z. Q. Mao, Y. Maeno, and Y. Liu, Science **306**, 1151 (2004).
[10]F. Kidwingira, J. D. Strand, D. J. Van Harlingen, and Y. Maeno, Science **314**, 1267 (2006).
[11]M. Matsumoto, J. Phys. Soc. Jpn. **68**, 994 (1999).
[12]H. Bluhm, Phys. Rev. B **76**, 144507 (2007).
[13]V. O. Dolocan, C. Veauvy, F. Servant, P. Lejay, K. Hasselbach, Y. Liu, and D. Mailly, Phys. Rev. Lett. **95**, 097004 (2005).
[14]J. R. Kirtley, C. Kallin, C. W. Hicks, E. A. Kim, Y. Liu, K. A. Moler, Y. Maeno, and K. D. Nelson, Phys. Rev. B **76**, 014526 (2007).
[15]C. W. Hicks, J. R. Kirtley, T. M. Lippman, N. C. Koshnick, M. E. Huber, Y. Maeno, W. M. Yuhasz, M. B. Maple, and K. A. Moler, Phys. Rev. B **81**, 214501 (2010).
[16]P. G. Bjornsson, Y. Maeno, M. E. Huber, and K. A. Moler, Phys. Rev. B **72**, 012504 (2005).
[17]M. Ichioka, Y. Matsunaga, and K. Machida, Phys. Rev. B **71**, 172510 (2005).
[18]T. M. Riseman, P. G. Kealey, E. M. Forgan, A. P. Mackenzie, L. M. Galvin, A. W. Tyler, S. L. Lee, C. Ager, D. M. Paul, C. M. Aegerter, R. Cubitt, Z. Q. Mao, T. Akima, and Y. Maeno, Nature (London) **396**, 242 (1998).
[19]C. M. Aegerter, S. H. Lloyd, C. Ager, S. L. Lee, S. Romer, H. Keller, and E. M. Forgan, J. Phys. Condens. Matter **10**, 7445 (1998).
[20]R. Heeb and D. F. Agterberg, Phys. Rev. B **59**, 7076 (1999).
[21]C. Kallin and A. J. Berlinsky, J. Phys. Condens. Matter **21**, (2009).
[22]Y. Liu, New J. Phys. **12**, 075001 (2010).
[23]Y. Maeno, S. Nishizaki, K. Yoshida, S. Ikeda, and T. Fujita, J. Low Temp. Phys. **105**, 1577 (1996).
[24]Z. Q. Mao, Y. Maeno, and H. Fukazawa, Mater. Res. Bull. **35**, 1813 (2000).
[25]V. V. Khotkevych, M. V. Milosevic, and S. J. Bending, Rev. Sci. Instrum. **79**, 123708 (2008).
[26]K. Hasselbach, V. O. Dolocan, P. Lejay, and D. Mailly, Phys. C (Amsterdam, Neth.) **460**, 277 (2007).
[27]J. Clem, J. Low Temp. Phys. **18**, 427 (1975).
[28]T. M. Riseman, P. G. Kealey, E. M. Forgan, A. P. Mackenzie, L. M. Galvin, A. W. Tyler, S. L. Lee, C. Ager, D. M. Paul, C. M. Aegerter, R. Cubitt, Z. Q. Mao, T. Akima, and Y. Maeno, Nature (London) **404**, 629 (2000).
[29]A. Gibbs (private communication).
[30]S. Raghu, A. Kapitulnik, and S. A. Kivelson, Phys. Rev. Lett. **105**, 136401 (2010).
[31] Huebener, *Magnetic flux structures in superconductors: Extended reprint of a classic text*, 2nd ed. (Springer, Berlin, 2001).
[32]V. Moshchalkov, M. Menghini, T. Nishio, Q. H. Chen, A. V. Silhanek, V. H. Dao, L. F. Chibotaru, N. D. Zhigadlo, and J. Karpinski, Phys. Rev. Lett. **102**, 117001 (2009).
[33]R. Gilardi, J. Mesot, A. J. Drew, U. Divakar, S. L. Lee, N. H. Andersen, J. Kohlbrecher, N. Momono, and M. Oda, Phys. C (Amsterdam, Neth.) **408**, 491 (2004).
[34]G. M. Luke, Y. Fudamoto, K. M. Kojima, M. I. Larkin, B. Nachumi, Y. J. Uemura, J. E. Sonier, Y. Maeno, Z. Q. Mao, Y. Mori, and D. F. Agterberg, Phys. B (Amsterdam, Neth.) **289-290**, 373 (2000).
[35]Y. Maeno, T. Ando, Y. Mori, E. Ohmichi, S. Ikeda, S. NishiZaki, and S. Nakatsuji, Phys. Rev. Lett. **81**, 3765 (1998).